(Received 16 June 2024, Accepted 19 July 2024, Scheduled 7 August 2024)

Conformal Angularly Stable Quadband Frequency Selective Surface for EMI Shielding

Naveena Meka and Krishnan Shambavi*

School of Electronics Engineering, Vellore Institute of Technology, Vellore, India

ABSTRACT: This article presents a miniaturized dual layer angularly stable quad-band frequency selective surface (FSS) for shielding applications. The shield consists of four metallic square rings on a thin FR4 substrate of relative permittivity 4.4 and thickness 0.5 mm with two rings on top layer and other two rings in the bottom layer. The dimension of the shielding unit cell is $0.2\lambda \times 0.2\lambda$, for the lowest frequency. These shields have been analyzed in both planar and conformal configurations. The equivalent circuit models as well as analytical model are determined. The shield exhibits quad band band-stop characteristics with transmission zeros at 5 GHz (4.3–5.8 GHz), 6.6 GHz (6.3–6.8 GHz), 8.3 GHz (7–8.8 GHz), and 15 GHz (11–17 GHz). These bands find their application in shielding upper WLAN band, sub-6 GHz 5G band C/Ku band for satellite communication. The proposed FSS prototype is fabricated and tested for shield effectiveness in an anechoic chamber. The proposed FSS design offers stable angular response up to 60° for planar and geometry. Simulated and measured transmission coefficients are in good agreement and hence well suited for shielding applications. As the structure is fourfold symmetric, it exhibits polarization insensitive and angular stability in all four bands.

1. INTRODUCTION

A periodic array of spatially filtering resonating elements known as Frequency Selective Surface (FSS) is used in the design of filters, absorbers, and radomes blocking unauthorized communication bands like GSM, Wi-Fi, Wi-Max, etc. and is necessary for information security. FSS with a stopband filter characteristic is an efficient option. The frequency filtering property of FSS is utilized in communication systems for antenna reflectors, hybrid radomes, spatial filters, and electromagnetic shelters. A high angular frequency selective surface-based spatial filter for dual-band (C- and X-bands) stop to block satellite downlink frequencies is proposed in [1]. The structure's unit cell consists of dipoles with two folded arms. The filter's transmission coefficient in the designated satellite frequency bands (3.7–4.2 GHz and 7.25–7.75 GHz) is less than −10 dB. The work [2] proposes a unique FSS structure for 28 GHz electromagnetic (EM) shielding, with vent holes covering more than 50% of the unit cell. It offers at least 30 dB attenuation for field illumination up to 60° (based on simulation) and a 2 GHz stopband to block undesired signals around 28 GHz in 5G NR. A Tri Band FSS [3] structure with copper patterns printed on both sides of the substrate exhibits minimal insertion loss.

A dual convoluted structure filtering at 2.66 GHz and 5 GHz is presented in [4] and has angular stability of 0, 30, 60 degrees. A two metallic layer Penta band-stop filter at PCS, Wi-Fi, CBRS, lower WLAN, and X-band downlink frequencies is observed in [5]. A single substrate dual layer with square loop and extended arms structure is implemented for triple band filtering in [6] which is used at WiMAX, WLAN, and X bands. An ultra-wide band stop response from 3.1 GHz to 13.1 GHz with single layer is proposed in [7]. A stopband FSS design for indoor application is suggested in [8] to shield the WLAN signals entering from outside environment. The structure provides polarization-independent response and demonstrates remarkable stability for oblique incidence angles. A triband band-stop frequency selective surface is used in the design to block the GSM 900, 1800, and Wi-Fi 2400 MHz frequency bands [9]. A 2.5-D ultra-miniaturized frequency selective surface (FSS) with two arbitrarily and independently adjustable stopbands is designed and analysed in [10]. These two stopbands can be separated into two separate wide bands or moved quite far apart. This novel FSS has just one dielectric layer that is printed on both sides, linking vertical via arrays with thin meandering lines. An FSS of ultra-thin applicable to X-band is presented in [11]. At 8.47 and 10.45 GHz, the proposed single-layer FSS functions as a band reject filter. A brand-new FSS with miniaturization having a band-stop response at 1.6 GHz is designed [12]. The planar FSS has convoluted components connected through via holes, thereby increasing the electrical length. A dual-band miniaturized second-order band-pass FSS is provided in [13]. A two-dimensional periodic array of double square loops and an array of wire grids are used to implement the design. The suggested structure, which consists of two dielectric layers and three metal layers, functions as a spatial dual-band microwave filter with a wide band separation. The tri-band FSS for rejecting GSM frequency bands is realized synthetic resonators [14].

In this paper, a quad-band band-stop miniaturized conformal frequency selective surface with good angular stability is designed, implemented, and tested. The four stopbands are

* Corresponding author: Krishnan Shambavi (kshambavi@vit.ac.in).

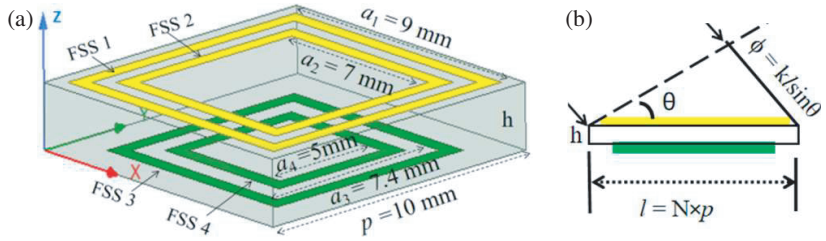

FIGURE 1. (a) Geometry of quad band stop FSS. (b) Maximum phase difference for oblique incidence.

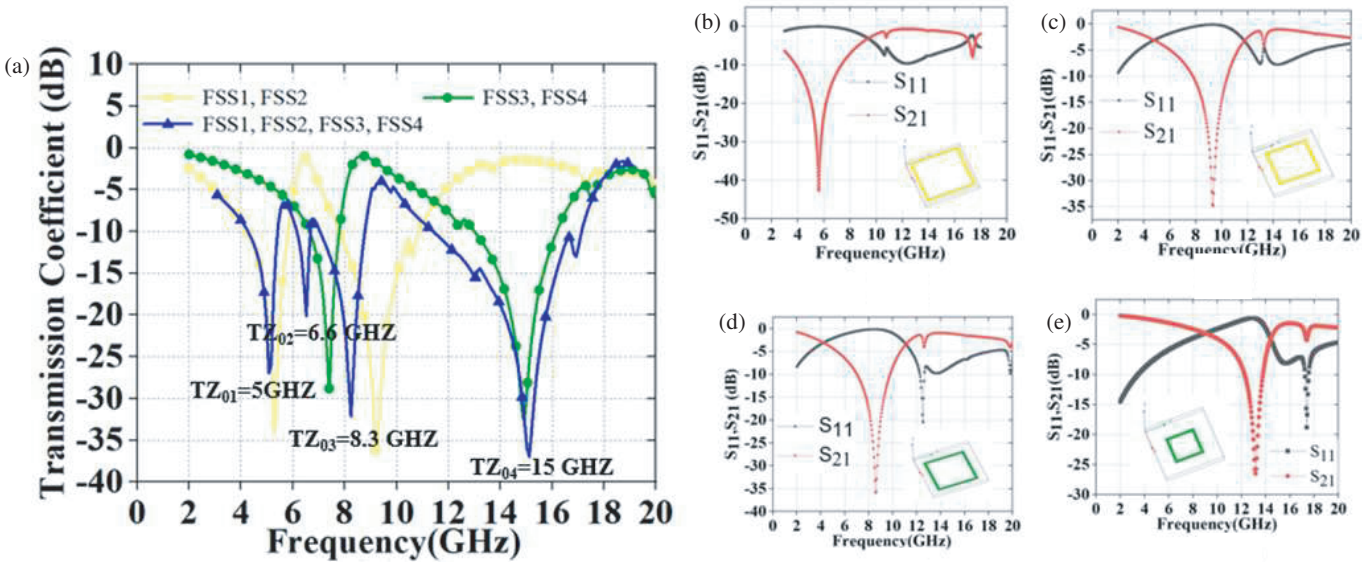

FIGURE 2. Transmission characteristics. (a) Combined FSS. (b) FSS 1. (c) FSS 2. (d) FSS 3. (e) FSS 4.

closely spaced with bandwidths 4.3–5.8 GHz, 6.3–6.8 GHz, 7–8.8 GHz, 11–17 GHz for shielding upper WLAN, sub-6 GHz band, C/Ku band of satellite communication. This paper is organized as follows. Section 2 describes the design and simulation of unit cell and 15×15 array followed by Section 3 about analysis for polarization and angular stability and Section 4 about measurement and testing.

2. DESIGN OF QUAD BAND FSS

2.1. Quadband Unit Cell

A schematic representation of unit cell configuration of the quad-band FSS array is depicted in Fig. 1. The unit cell is realized on an epoxy glass FR4 substrate ($\varepsilon_r = 4.4$ and $\tan\delta = 0.01$ and thickness $h = 0.5$ mm). Top and bottom layers consist of two square metallic rings resonating at different stop band frequency. Stopband resonant frequency depends on its square ring side length (a_n) and width (w) of the ring as given in (1).

$$f = \frac{\lambda}{8(a_n - w)} \tag{1}$$

As shown in Fig. 1(b) at oblique incidence angle (θ), maximum phase delay due to phase difference, ϕ, is introduced during excitation which in turn depends on the periodicity, p, of a unit cell, phase constant ($k = 2\pi/\lambda$, and total length of an array l. For an $N \times N$ element array, the maximum phase difference introduced is given by (2). The shift in the resonant frequency due to phase delay can be controlled by the proper selection of unit cell size which in turn limits the grating lobe appearance frequency f_g (3), where c is the wave velocity in the free space medium. For $\theta = 60°$ and $f_g = 26$ GHz, the periodicity $p = 10.14$ mm from (2) and (3). The proposed quad-band FSS stopband response is well below the grating lobe frequency. High Frequency Structure Simulator (HFSS) is used for the simulation of the proposed quad-band FSS.

$$\phi = kl\sin\theta \tag{2}$$

$$f_g = \frac{c}{\lambda_g} = \frac{c\sqrt{\varepsilon_{eff}}}{p(1+\sin\theta)} \tag{3}$$

2.2. Evolution of Quad-Band FSS Unit Cell

When FSS is realised as an individual resonator, the transmission zeros occur at 5.61 GHz, 9.33 GHz, 8.5 GHz,and 13.43 GHz for the FSS structures 1, 2, 3, and 4, respectively.

When FSS 1, FSS 2, FSS 3, FSS 4 are combined, due to mutual coupling effect the electrical length of the resonator varies which in turn shifts the transmission zero frequency with slight

TABLE 1. Resonant frequency comparison (evolution of quad-band FSS unit cell).

FSS 1 f_{01} (GHz)	*FSS 2* f_{02} (GHz)	*FSS 3* f_{03} (GHz)	*FSS 4* f_{04}(GHz)
5.61 (4.19–5.8 GHz)	9.33 (7.85–10.91 GHz) FSS2	8.5 (6.74–7.88 GHz) FSS3	13.43 (12.9–16.9 GHz) FSS4
(Combined FSS 1, FSS 2)		*(Combined FSS 3, FSS 4)*	
f_{01} (GHz)	f_{02} (GHz)	f_{03} (GHz)	f_{04} (GHz)
5.3 (4.2–5.8 GHz)	9.2 9.78–10.8 GHz)	7.5 (6.6–7.7 GHz)	14.8 (13–16 GHz)
(Combined FSS 1, FSS 2, FSS 3, FSS 4)			
f_{01} (GHz)	f_{02} (GHz)	f_{03} (GHz)	f_{04} (GHz)
5 (4.3–5.8 GHz)	8.3 (7.0–8.8 GHz)	6.6 (6.3–6.8 GHz)	15 (11–17 GHz)

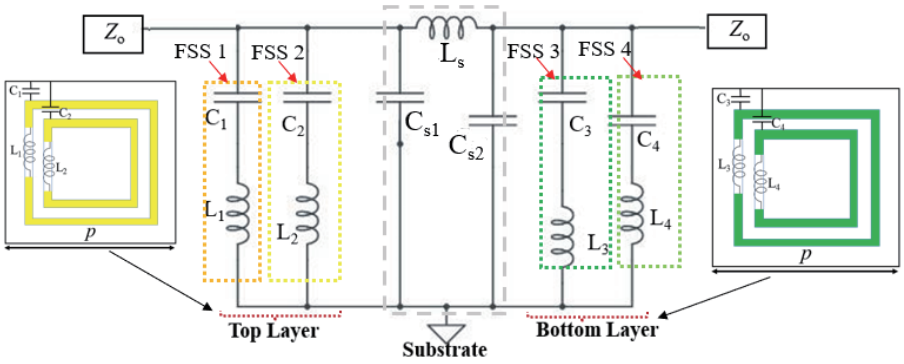

FIGURE 3. Equivalent circuit model of the quad band unit cell. ($C_1 = 0.03$ pF, $L_1 = 5.5$ nH, $C_2 = 0.03$ pF, $L_2 = 17$ nH,$C_3 = 0.06$ pF, $L_3 = 3.4$ nH, $C_4 = 0.025$ pF, $L_4 = 3$ nH, $L_s = 1.2$ nH, $C_{s1} = 0.03$ pF, $C_{s2} = 0.04$ pF, $Z_o = 377\,\Omega$).

change in the bandwidth. Band-stop frequency and bandwidth of an individual FSS and combined FSS are clearly depicted in Fig. 2 and Table 1.

2.3. Equivalent Circuit of Quad-Band FSS

The Equivalent Circuit Model (ECM) of the quad-band FSS provides deeper insight to the physical principles of FSS under quasi-static conditions. Fig. 3 shows the ECM of quad-band FSS under a normally incident EM wave with electric field polarization along x axis.

FSS on each layer can be modelled as a series combination of inductance (L) and capacitance (C). The inductor (L_n) and capacitor (C_n) values can be calculated using the formulas given below.

$$L_t = \mu\left(\frac{l}{2\pi}\right)\log\left[\csc\left(\frac{\pi W}{2l}\right)\right] \tag{4}$$

$$C_t = \varepsilon_{eff}\varepsilon_o\frac{2p}{\pi}\log\left[\csc\left(\frac{\pi S}{2p}\right)\right] \tag{5}$$

where l and w are the length and width of the FSS ring; p is the periodical length of proposed FSS; and s is the gap width between edges of two adjacent metallic rings. Effective permittivity of the substrate, ε_{eff}, can be calculated as

$$\varepsilon_{eff} = \frac{\varepsilon_r + 1}{2} \tag{6}$$

FR4 substrate is a transmission line stub which can be replaced by a high impedance line of 0.11 rad length and impedance of 179 Ω. Inductance and capacitance L_s, C_{s1}, C_{s2} of the short section transmission line can be calculated as

$$L_s = \mu_o\mu_r h \tag{7}$$

$$C_s = \frac{\varepsilon_o\varepsilon_r h}{2} \tag{8}$$

ε_o and μ_o represent the permittivity and permeability of free space. Semi-infinite free space medium on either side of quad-band FSS is represented by free space impedance Z_o. Transmission feature of FSS equivalent circuit can be analysed using two-port network parameters. ABCD matrix of the FSS circuit can be expressed as

$$\begin{pmatrix} A & B \\ C & D \end{pmatrix} = (M_{\text{FSS}})(M_s) = \begin{pmatrix} 1 & 0 \\ \frac{1}{Z_{\text{FSS}}} & 1 \end{pmatrix}\begin{pmatrix} \cos(kh) & j\sin khz_o \\ j\frac{\sin(kh)}{Z_o} & \cos(kh) \end{pmatrix} \tag{9}$$

where M_{FSS} is the scattering matrix of FSS structure, and M_s is the scattering matrix of the dielectric layer. Z_{FSS} is the impedance of FSS structure, and it depends on the incident frequency and the medium parameters. For TE mode $Z_{\text{FSS}} = \omega\mu_o\mu_r/k$, and for TM mode $Z_{\text{FSS}} = k/\omega\varepsilon_o\varepsilon_r$. Transmission coefficient of FSS can be expressed as

$$S_{21}=\frac{2Z_o}{AZ_o+B+CZ_o^2+DZ_o} \tag{10}$$

From (9) and (10) at normal incidence and for oblique incidence angle up to 60°, the transmission coefficient is almost zero, and it occurs when inductive and capacitive reactances cancel out each other. The frequency at which the transmission is zero is given as

$$f_n=\frac{1}{2\pi\sqrt{\varepsilon_{eff}L_n}(C_n+C_{sm})} \tag{11}$$

Figure 4 shows the transmission response of the ECM implemented in ADS software and its comparison with HFSS. It can be inferred that the frequency response characteristics remains the same.

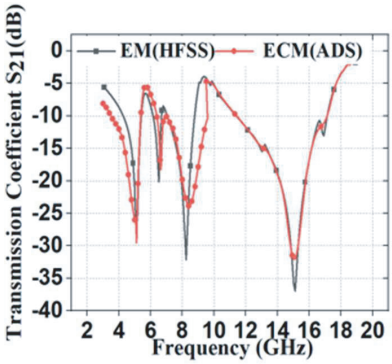

FIGURE 4. Comparison of simulated and ADS transmission response.

2.4. Quad Band Array (15 × 15)

The geometry of proposed quad-band FSS array is shown in Fig. 5. Transmission response of unit cell and 15 × 15 array remains the same, shown in Fig. 6.

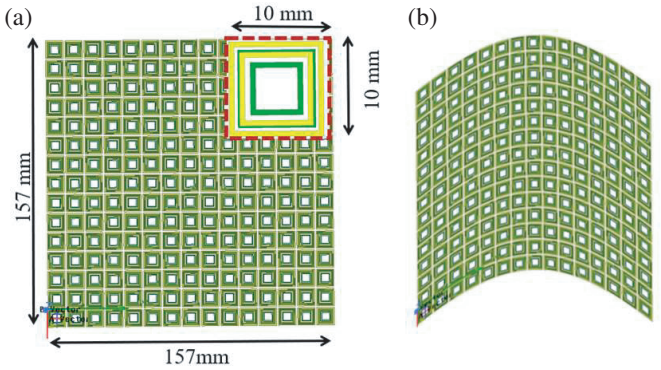

FIGURE 5. Geometry of the proposed (a) planar FSS array, (b) conformal FSS array.

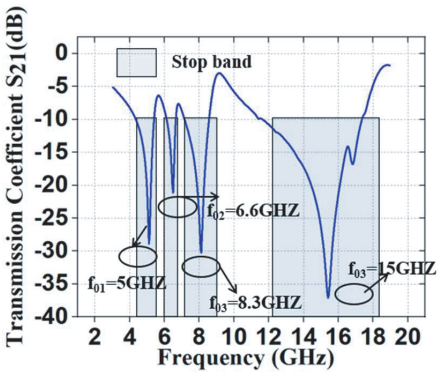

FIGURE 6. Transmission response of proposed quad band stop 15 × 15 FSS Array.

3. SIMULATION RESULTS

3.1. Stop Band Filter Characteristics

To describe the band-stop filter mechanism, surface current distribution at the respective band-stop resonant frequency for TE mode is shown in Fig. 7. At 5 GHz band-stop frequency, maximum current is distributed on the top outer ring (FSS1) while very weak current is distributed in other FSS2, FSS3, FSS4. Similarly at 6.6 GHz stopband frequency of FSS2, 8.3 GHz stopband frequency of FSS3 and 15 GHz stopband frequency of FSS4, maximum current is distributed in their respective FSS resonance structure, and very weak current is distributed in all other FSS structures.

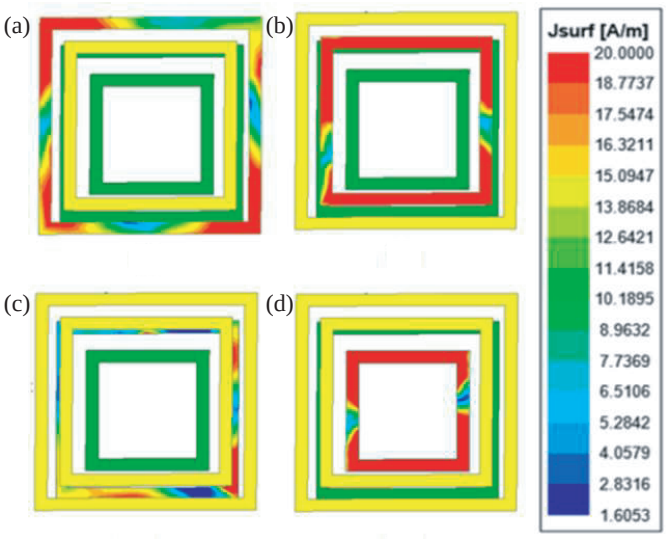

FIGURE 7. Surface current distribution of proposed Quad-band band stop FSS for TE mode at frequencies. (a) 5 GHz, (b) 6.5 GHz, (c) 8.3 GHz, (d) 15 GHz.

3.2. Angular Stability

Figures 8(a) and (b) show the transmission response of quad-band band-stop FSS for different angles of incidence. It is observed that the quad-band FSS exhibits stable frequency response characteristics for both normal and oblique incidence angles up to 60° in elevation and azimuthal plane. Stability can

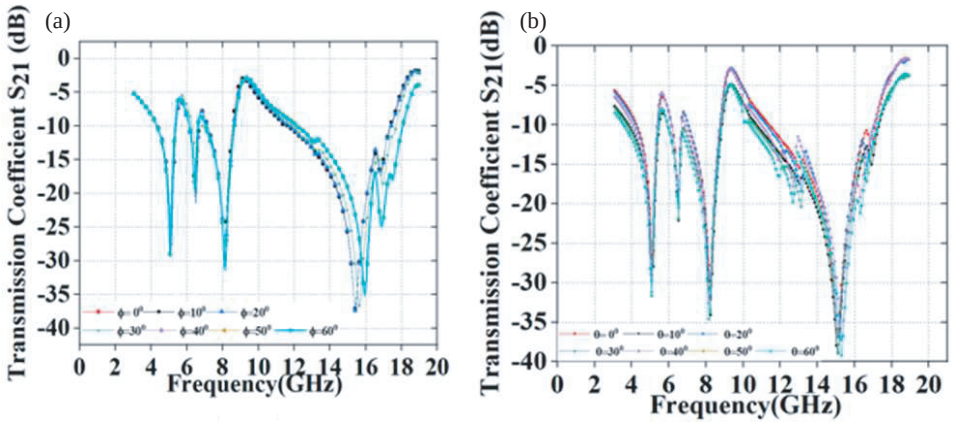

FIGURE 8. Transmission response of quad band band-stop FSS for different angles of incidence (a) Phi, (b) theta.

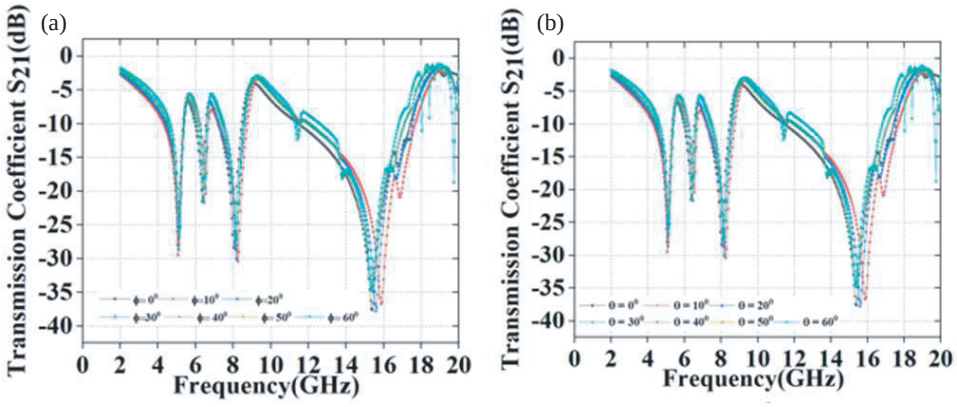

FIGURE 9. Transmission response of (a) TE Mode, (b) TM Mode.

also be analyzed with Figure of Merit which is defined by

$$\text{Figure of Merit } = \frac{2|\text{FBW}\,(\theta_{\max}) - \text{FBW}\,(\theta_{\min})\,|}{\text{FBW}\,(\theta_{\max}) - \text{FBW}\,(\theta_{\min})} \tag{12}$$

As the geometry is symmetric, the transmission coefficient response for all the angles of theta and phi up to 60° remains the same. FBW is the fractional bandwidth for maximum incidence angle ($\theta_{\max}$) and minimum incidence angle ($\theta_{\min}$). As per (12), the values of Figure of Merit for the quad bands are 0.72, 0.09, 0.8, and 0.66 which indicates its angular stability.

3.3. Polarization Stability

Transmission response of the quad-band FSS for different incidence angles of TE and TM polarizations is shown in the Figs. 9(a) and (b). In TE mode FSS array exhibits stability up to 60 degrees without affecting the quad-band stopband frequency and bandwidth. Beyond 60-degree, transmission zero shifts to lower frequency, and bandwidth decreases (Table 1). In TM mode there is 0.5% resonance shift in the fourth band at 60 degrees. The mode impedance is related to incidence angle by $Z_{\text{TE}} = Z_o/\cos\theta$ and $Z_{\text{TM}} = Z_o\cos\theta$. The increase in incidence angle results in Z_{TE}, Z_{TM} variation, by affecting the quality factor. Beyond 60-degree transmission zero frequency shifts to upper frequency. Because of the four-fold symmetric geometry, transmission coefficient response is identical for TE and TM modes up to 60°.

3.4. Shield Effectiveness (SE)

Shielding ability of a structure is given by Shielding Effectiveness (13), where E_t is the transmitted electric field, and E_i is the incident electric field. SE can also be calculated from S_{21} transmission parameters as given in (13)

$$SE\,(\text{dB}) = -20\log\left|\frac{Et}{Ei}\right| = -S_{21}\,(\text{dB}) \tag{13}$$

$$SE = -20\log\frac{S_{21\text{WFSS}}}{S_{21\text{WoFSS}}} \tag{14}$$

where $S_{21\text{FSS}}$ and $S_{21\text{WoFSS}}$ are the simulated S_{21} with and without FSS array structure. Simulated SE for phi and theta variation is shown in Figs. 10(b) and (c). Because of the four-fold symmetric geometry, SE remains the same for both TE and TM polarizations at normal and up to 60° oblique incidence angles. SE at four transmission zeros is 30 dB, 23 dB, 34 dB, and 38 dB.

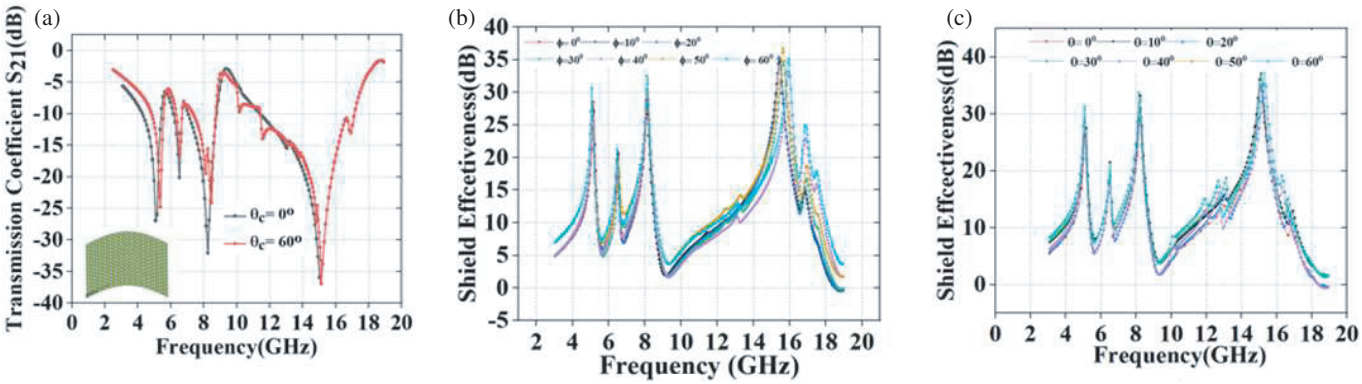

FIGURE 10. Conformal FSS array response. (a) Transmission coefficient. (b) SE for Phi Variation. (c) SE for Theta Variation.

TABLE 2. Comparison of proposed work to previous work.

Ref	Size(mm^2)	Frequency (GHz)	Periodicity (λ_p)	Angular stability
[4]	6.8×6.8	2.6,5	0.045	60°
[5]	10.7×10.7	1.9, 2.4, 3.6, 5.4, 7.5	0.067	54°
[6]	10×10	3.5, 5.2, 10.2	0.011	50°
[7]	10×10	6.8	0.226	45°
[8]	7×7	5	0.116	60°
[9]	26×26	0.9, 1.8, 2.4	0.078	60°
[10]	6.2×6.2	1.7, 3.6	0.035	85°
[11]	8.8×8.8	8.1, 10.3	0.23	60°
This work	**10×10**	**5, 6.6, 8.3, 15**	**0.2**	**60°**

3.5. Conformal FSS

The thin profile of the quad-band FSS array exhibits its pertinence on a conformal surface. Radius of the curved surface for a conformal angle θ_c is given by $R_C = 180l/\pi\theta_c$ where l is the arc length. To analyze the effects of conformal factors on the transmission characteristics, 15×15 array was placed on a cylindrical surface and evaluated for different radii of curvature (Fig. 10(a)). It can be observed that as the radius of the cylinder decreases, the transmission zero shifts to higher frequency, and bandwidth remains almost stable.

4. MEASURED RESULTS

To validate the proposed design concept, a prototype containing an array of 15×15-unit cells was fabricated over an FR4 substrate of thickness 0.5 mm using chemical etching process. A photograph of this fabricated prototype is shown in Fig. 11(a). Transmission characteristics of proposed quad-band FSS were measured in an anechoic chamber using standard horn antennas (ETS 3115 double rigid horn antenna) connected to key sight 9374A vector network analyser using free space measurement technique. To reduce the edge effect, the proposed FSS prototype has been enveloped with microwave absorbers. Fig. 11(b) shows the measurement setup for transmission characteristics at normal incidence. The distance between the FSS array sample and the antenna is 1 metre. To ensure the accuracy, the transmission coefficient and shield effectiveness for TE and TM was measured first without sample and next with FSS prototype placed between the standard horn antennas. The difference was taken to mitigate the influence of the chamber environment and test systems. Fig. 12 depicts that the measured SE is in good agreement with the simulated results, and the proposed quad-band FSS blocks EM wave frequency ranging from 4.3–4.8 GHz, 6.3–6.8 GHz, 7.0–8.8 GHz, 11–17 GHz which are responsible for WLAN frequency, satellite, C and

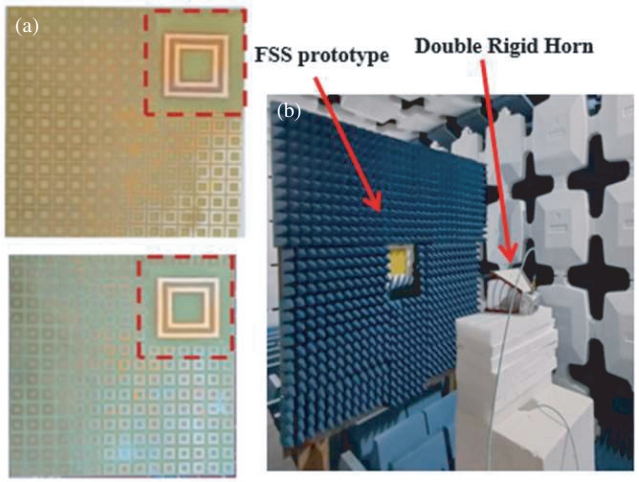

FIGURE 11. (a) Top and bottom view of fabricated prototype. (b) Measurement setup.

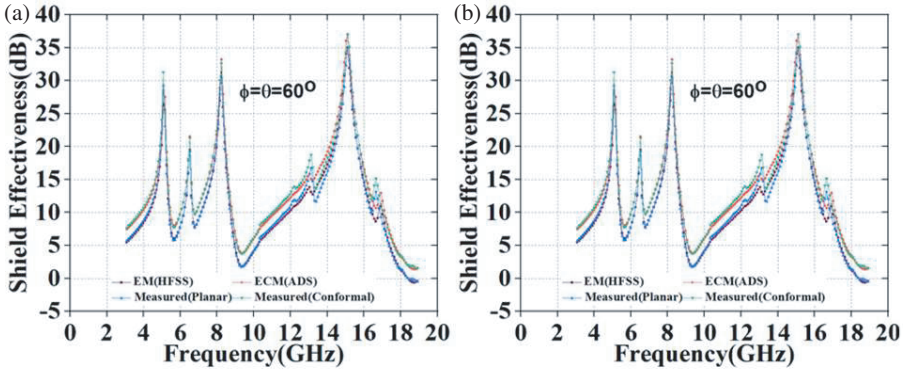

FIGURE 12. Comparison of measured and simulated results of quad band FSS array for incidence angle. (a) 0°. (b) 60°.

Ku band applications. As the structure is fourfold symmetric, it also exhibits similar characteristics for oblique incidence.

A comparison of the proposed quad-band FSS and other multi-band FSS characteristic designs in the literature is tabulated in Table 2. The proposed FSS exhibits quad band shielding with polarization and better angular stability characteristics in both planar and conformal configurations, and its size is smaller than [4] to [11]. The proposed FSS also exhibits polarization insensitive and better angular stability characteristics at all bands up to 60 degrees in both planar and conformal configurations.

5. CONCLUSION

In this paper, a dual-layer conformal angularly stable quad-band band-stop FSS for shielding applications is proposed. In order to verify the performance of proposed FSS, a prototype is fabricated and tested for shielding characteristics. FSS exhibits band-stop resonance at 5 GHz, 6.6 GHz, 8.3 GHz, and 15 GHz with stopband bandwidths of 4.3–5.8 GHz, 6.3–6.8 GHz, 7–8.8 GHz, 11–17 GHz. Shield effectiveness of minimum 23 dB and maximum 38 dB is achieved. The designed FSS provides good angular and polarization stability up to 60 degrees for both planar and conformal structures. Hence, the proposed quad-band FSS can be used for shielding upper WLAN band, sub-6 GHz 5G band and C/Ku band of satellite communication. The proposed design can be further optimized for shielding multi-bands of wireless spectrum.

REFERENCES

[1] Venkatesh, G., M. Thottappan, and S. P. Singh, "Highly angularly stable dual-band stop FSS for blocking satellite downlink frequencies," *IEEE Transactions on Electromagnetic Compatibility*, Vol. 64, No. 6, 2055–2059, Dec. 2022.

[2] Yan, L., L. Xu, R. X.-K. Gao, J. Zhang, X. Yang, and X. Zhao, "Angularly independent frequency selective surface with good ventilation for millimeter wave EM shielding," *IEEE Transactions on Electromagnetic Compatibility*, Vol. 64, No. 1, 251–254, Feb. 2022.

[3] Shah, G., Q. Cao, Z. U. Abidin, and Z. Rafique, "A hybrid element triband frequency selective surface with high angular stability and polarization insensitivity," *IEEE Transactions on Electromagnetic Compatibility*, Vol. 62, No. 6, 2759–2764, Dec. 2020.

[4] Ma, Y., W. Wu, Y. Yuan, X. Zhang, and N. Yuan, "A convoluted structure for miniaturized dual-bandstop frequency selective surface," *IEEE Antennas and Wireless Propagation Letters*, Vol. 18, No. 2, 328–332, Feb. 2019.

[5] Ghosh, A., M. Kumar, S. N. Islam, and S. Das, "Design and analysis of a compact penta-band polarization-insensitive bandstop frequency selective surface," *IEEE Antennas and Wireless Propagation Letters*, Vol. 19, No. 1, 59–63, Jan. 2020.

[6] Bashiri, M., C. Ghobadi, J. Nourinia, and M. Majidzadeh, "WiMAX, WLAN, and X-band filtering mechanism: Simple-structured triple-band frequency selective surface," *IEEE Antennas and Wireless Propagation Letters*, Vol. 16, 3245–3248, 2017.

[7] Sampath, S. S. and R. Sivasamy, "A single-layer UWB frequency-selective surface with band-stop response," *IEEE Transactions on Electromagnetic Compatibility*, Vol. 62, No. 1, 276–279, Feb. 2020.

[8] Natarajan, R., M. Kanagasabai, S. Baisakhiya, R. Sivasamy, S. Palaniswamy, and J. K. Pakkathillam, "A compact frequency selective surface with stable response for WLAN applications," *IEEE Antennas and Wireless Propagation Letters*, Vol. 12, 718–720, 2013.

[9] Kumar, T. R. S. and K. J. Vinoy, "A miniaturized angularly stable FSS for shielding GSM 0.9, 1.8, and Wi-Fi 2.4 GHz bands," *IEEE Transactions on Electromagnetic Compatibility*, Vol. 63, No. 5, 1605–1608, Oct. 2021.

[10] Wei, P.-S., C.-N. Chiu, and T.-L. Wu, "Design and analysis of an ultraminiaturized frequency selective surface with two arbitrary stopbands," *IEEE Transactions on Electromagnetic Compatibility*, Vol. 61, No. 5, 1447–1456, Oct. 2019.

[11] Ünaldı, S., S. Çimen, G. Çakır, and U. E. Ayten, "A novel dual-band ultrathin FSS with closely settled frequency response," *IEEE Antennas and Wireless Propagation Letters*, Vol. 16, 1381–1384, 2016.

[12] Sampath, S. S., R. Sivasamy, and K. J. J. Kumar, "A novel miniaturized polarization independent band-stop frequency selective surface," *IEEE Transactions on Electromagnetic Compatibility*, Vol. 61, No. 5, 1678–1681, Oct. 2019.

[13] Yan, M., S. Qu, J. Wang, A. Zhang, L. Zheng, Y. Pang, and H. Zhou, "A miniaturized dual-band FSS with second-order response and large band separation," *IEEE Antennas and Wireless Propagation Letters*, Vol. 14, 1602–1605, 2015.

[14] Kartal, M., J. J. Golezani, and B. Doken, "A triple band frequency selective surface design for GSM systems by utilizing a novel synthetic resonator," *IEEE Transactions on Antennas and Propagation*, Vol. 65, No. 5, 2724–2727, May 2017.